PCCP

PAPER

Electrocatalytic oxygen reduction kinetics on Fe-center of nitrogen-doped graphene†

Cite this: *Phys. Chem. Chem. Phys.*, 2014, **16**, 13733

Jing Sun,[a] Ya-Hui Fang[ab] and Zhi-Pan Liu*[a]

The Fe/N/C catalysts have emerged recently as a representative class of non-Pt catalysts for oxygen electrocatalytic reduction, which could have a competitive catalytic performance to Pt. However, the nature of the catalyst remains elusive, especially on the active site structure and the electrocatalytic kinetics. Here we examine two kinds of Fe/N active sites for Fe/N/C catalysts, namely, the four-coordinated FeN_4 and the five-coordinated $Fe(CN)N_4$ centers embedded in graphene layers. By using large-scale first principles calculations with a periodic continuum solvation model based on the Modified-Poisson–Boltzmann equation (CM-MPB), we identified the four (4e) and two electron (2e) oxygen reduction pathways under acidic conditions. We find that both 4e and 2e pathways involves the formation of an OOH intermediate, which breaks its O–OH bond in the 4e pathway but is reduced to H_2O_2 in the 2e pathway. We show that at 0.8 V *vs.* SHE, the 4e pathway is preferred at both FeN_4 and $Fe(CN)N_4$ centers, but the 2e pathway is kinetically also likely on the $Fe(CN)N_4$ center. The O–OH bond breaking of OOH is the key kinetic step, which has a similar free energy barrier to the OH reduction on the FeN_4 center, and is the rate-determining step on the $Fe(CN)N_4$ center. Due to the high adsorption energy of Fe towards the fifth ligand, such as OH and CN, we expect that the active site of the real Fe/N/C catalyst is the five coordinated Fe center. We found that the barrier of the O–OH bond breaking step is not sensitive to potential and a Tafel slope of 60 mV is predicted for the ORR on the $Fe(CN)N_4$ center, which is consistent with experimental observation.

Received 5th January 2014,
Accepted 27th February 2014

DOI: 10.1039/c4cp00037d

www.rsc.org/pccp

1. Introduction

The oxygen reduction reaction (ORR, $O_2 + 4H^+ + 4e \rightarrow 2H_2O$) is a key electrocatalytic reaction for fuel cell applications, which converts O_2 to water using proton and electrons at the cathode. To date, the most widely used catalysts for ORR are still the expensive Pt and Pt-based alloys[1–3] and great efforts have been devoted to search for non-Pt catalysts aiming to overcome the high overpotential and the long-term stability problems of traditional catalysts. Since Jasinski and coworkers found that metal phthalocyanines featuring a metal–N_4 center are able to catalyze ORR under acidic conditions,[4] recent years have seen encouraging progress to immobilize the metal–N complex (mainly Fe–N^{5-8}) and also to improve its catalytic performance. For example, such active catalysts can be synthesized by simply heating common nitrogen containing chemicals, Fe inorganic salts and carbon black.[9–11] Due to the complex nature of the catalysts, the atomic structure of the active site and the catalytic mechanism of these metal/N/C catalysts remain largely elusive.

Because the Fe macrocycles such as porphyrin and phthalocyanine are catalytically active for the ORR,[12–17] the basic structural motif, *i.e.* Fe–N_4, has been regarded to be the active center in the heterogeneous environment as well. The presence of metal–N_4 like FeN_4, CoN_4 moiety was indeed detected by various experimental techniques.[18–23] For example, Dodelet *et al.* using Time of Flight Secondary Ion Mass Spectrometry detected FeN_4 species in the catalyst prepared using Fe acetate, Fe porphyrin and NH_3 as the precursor.[24,25] Koslowski related the current density of ORR to the amount of in-plane FeN_4 centers using Mössbauer spectra and a linear correlation was identified.[18] Thermodynamics analysis using first principles calculations also indicated that the FeN_4 embedded in graphene could be active for ORR.[26,27] On the other hand, newly emerging evidence suggests that the metal–N_4 might not be exactly the active site: the chemical environment around this center could also affect significantly the ORR activity. It was demonstrated that the presence of the porosity in the pristine carbon black during the pyrolysis (*e.g.* using disordered carbon) is important for achieving high catalytic activity.[28,29] This implies that the active site forms at/near the micropores of the nitrogenized

[a] *Shanghai Key Laboratory of Molecular Catalysis and Innovative Materials, Key Laboratory of Computational Physical Science (Ministry of Education), Department of Chemistry, Fudan University, Shanghai 200433, China. E-mail: zpliu@fudan.edu.cn*

[b] *School of Chemical and Environmental Engineering, Shanghai Institute of Technology, Shanghai 201418, China*

† Electronic supplementary information (ESI) available. See DOI: 10.1039/c4cp00037d

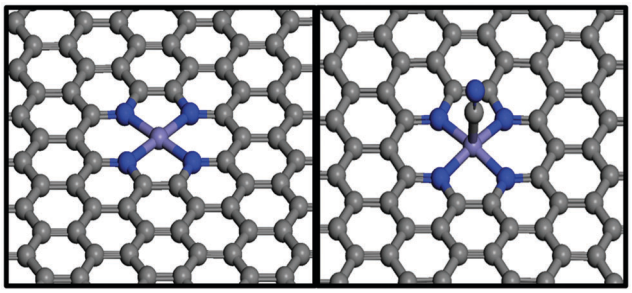

Fig. 1 Two possible active sites embedded in the graphene sheet modeled in this study. Left: the four-coordinated planar FeN_4 center; Right: the five-coordinate square-pyramidal $Fe(CN)N_4$ center. The grey, blue and purple balls represent C, N and Fe, respectively.

graphite. Instead of the four-coordinated Fe center, the five-coordinated Fe center was also suggested by Jain *et al.*,[30] the structure of which mimics the Fe–porphyrin complex in biological systems for O_2 activation.[31,32]

In this work, we aim to understand the mechanism and the kinetics of the Fe center catalyzed ORR on the nitrogen-doped graphite by using first principles calculations. Two different models for the Fe center, namely, a four-coordinated FeN_4 center and a five coordinated $Fe(CN)N_4$ center on graphene have been considered as the possible active sites. The CN ligand is chosen as the fifth ligand because the CN ions has been well detected in the synthesis of Fe/N/C catalysts at high temperature.[9] The structures of these two models are as shown in Fig. 1.

2. Calculation methods and models

All DFT calculations were performed using the SIESTA package with numerical atomic orbital basis sets and Troullier–Martins norm conserving pseudopotentials.[33–35] The exchange–correlation functional utilized was at the generalized gradient approximation level, known as GGA-PBE.[36] A double-ξ plus polarization basis (DZP) set was employed. The orbital-confining cutoff was determined from an energy shift of 0.010 eV. The energy cutoff for the real space grid used to represent the density was set as 250 Ry. The Quasi-Newton Broyden method was employed for geometry relaxation until the maximal forces on each relaxed atom were less than 0.1 eV $Å^{-1}$. To correct the zero-point energy (ZPE), the vibrational frequency calculations were performed *via* the finite-difference approach. Transition states (TSs) of the catalytic reaction were located using the Constrained-Broyden based methods developed recently in this group and were verified using the vibrational frequency calculation.[37,38] The convergence of the key results with respect to the force criterion have been checked by reducing the criterion to be as low as 0.02 eV $Å^{-1}$, and the calculated adsorption energy (*e.g.* O_2 adsorption) and the barrier (*e.g.* O_2H^* dissociation) are found to be different by less than 0.05 eV.

The solid/liquid interface is modeled using the periodic continuum solvation model based on the modified Poisson–Boltzmann equation (CM-MPB), which can take into account the long-range electrostatic interaction due to solvation. The short-range solvation effect has been considered by adding the explicit water molecules as the first solvation shell. The periodic DFT/CM-MPB method has been utilized in our previous work on electro-/photocatalysis, where the detail of the implementation of the method is described.[39,40]

To derive the free energy reaction profile, we first obtain the reaction energy of each step (strictly speaking, Helmholtz free energy change (ΔF) at 0 K, 0 bar) that is directly available from DFT total energy (ΔE) after the ZPE correction. For elementary surface reactions without involving the adsorption/desorption of gaseous or liquid molecules, ΔF at 0 K, 0 bar is a good approximation to the Gibbs free energy (ΔG) as the temperature T and pressure p contributions at the solid phase are small. To compute the free energy change ΔG of elementary reactions involving gaseous or liquid molecules, such as oxygen, hydrogen, and water, the large entropy term at 298 K is essential to take into account. We utilize the standard thermodynamic data[41] to obtain the temperature and pressure contributions for the G of the aqueous H_2O and gaseous H_2, which are −0.57 eV (the entropy contribution is −0.22 eV in solution) and −0.31 eV compared to the total energy of the corresponding free molecule (E, 0 K), respectively.[42] The G of O_2 is derived as $G[O_2] = 4.92$ (eV) + $2G[H_2O] - 2G[H_2]$ by utilizing OER equilibrium at the standard conditions; the G of H_2O_2 is derived similarly considering that the H_2O_2/O_2 standard equilibrium potential is 0.682 V *vs.* SHE. For reactions involving the release of proton and electron, the reaction energy can be computed by referencing to the normal hydrogen electrode (SHE) in a manner proposed by the groups of Bockris[43] and Nørskov.[44] This is governed by $G_{\text{proton+electron}} = G(1/2H_2) - neU$, where e presents the transfer electron, n means the number of electrons, and U is the electrochemical potential *vs.* SHE. The other detail for computing the reaction kinetics of ORR under electrochemical conditions is as described in our previous work for ORR on Pt surfaces.[45]

To study the ORR mechanism on the Fe/N/C catalysts, here we propose two possible types of active centers, namely, the four coordinated planar FeN_4 center (pyridine-like structure for each N), and the five-coordinated square-pyramidal $Fe(CN)N_4$, as shown in Fig. 1. The planar FeN_4 is embedded in the graphene plane, which can be considered by substituting six C atoms of the graphene by one Fe and four N atoms. It should be mentioned that the exact structure of the active site for ORR in Fe/N/C catalysts is not known. Due to the high temperature condition in the synthesis (*e.g.* typically 900 °C[46]), HCN and CN ions have been detected in experiment by reacting NH_3 with carbon[47] and it is thus possible that the CN ion[21] acts as a ligand coordinated to the FeN_4 center. It should be emphasized that the $Fe(CN)N_4$ center cannot be held inside the graphite due to the large steric repulsion between the CN group and the neighboring layer of the graphite, but it may well be present at/near the micropores in real catalysts.

The FeN_4 and the $Fe(CN)N_4$ catalyst are modelled by embedding the active center in a graphene sheet with each unit cell containing 58 carbon atoms and a FeN_4 or $Fe(CN)N_4$ center. The unit cell utilized in this work is 17.04 × 9.84 Å with the vacuum region larger

than 30 Å. In this theoretical model, the Fe concentration is about 7 wt%, higher than that in the Fe/N/C catalysts reported in experiment with the best performance, *e.g.* from 0.02 wt% to 2 wt%,[21] but lower than that in the porphyrin molecule (15.38 wt%) that is known to be active for ORR in solution. The low Fe concentration of the Fe/N/C catalysts in experiment could be due to the difficulty of dispersing/incorporating single Fe ions into the graphite layers. Experimentally, the Fe concentration at the active site is limited by the microporous surface area, which is equivalent to Fe loading of ~1 wt%.[10]

3. Results and discussion

For ORR on Fe/N/C catalyst at the acidic conditions, the number of electron transfers measured with the Koutecky–Levich experiment is generally less than 4,[48] indicating that both 4e and 2e reduction occur simultaneously in ORR. It was believed that the 4e reduction involves sequentially the O_2*, OOH*, OH* and O* intermediates[23,26,27] (* indicates the adsorbed species) as every elementary step of the reaction is exothermic at 0 V *vs.* SHE as shown by thermodynamics calculations.[23] For the 2e reduction, it could involve OOH* and HOOH* intermediates (without O–O bond breaking) and H_2O_2 is as the final product.[49] The proposed mechanisms from the literature can be summarized as eqn (1)–(8). Eqn (1)–(6) are the 4e reduction pathway and eqn (7) and (8) are the 2e pathway. The OOH* intermediate appears in both pathways and thus is the key species determining the selectivity. The main purpose of the current work is to evaluate the potential-dependent reaction thermodynamics and kinetics of the 4e and 2e reduction pathways quantitatively on the graphene-embedded FeN_4 and $Fe(CN)N_4$ models in order to provide new insights into the working mechanism and the nature of the active site of the Fe/N/C catalyst.

$$O_2 \rightarrow O_2^* \quad (1)$$

$$O_2^* + H^+_{(aq)} + e^- \rightarrow OOH^* \quad (2)$$

$$OOH^* + H^+_{(aq)} + e^- \rightarrow O^* + H_2O \quad (3)$$

$$O^* + H^+_{(aq)} + e^- \rightarrow OH^* \quad (4)$$

$$OH^* + H^+_{(aq)} + e^- \rightarrow H_2O^* \quad (5)$$

$$H_2O^* \rightarrow H_2O_{(aq)} \quad (6)$$

$$OOH^* + H^+_{(aq)} + e^- \rightarrow HOOH^* \quad (7)$$

$$HOOH^* \rightarrow H_2O_{2(aq)} \quad (8)$$

3.1 Structure of the FeN center

The geometrical structure of the active sites was first investigated in a vacuum (without the applied electrochemical potential and the solvation). In the optimized structure for the FeN_4 embedded in the graphene sheet, the Fe was found to locate at the plane of graphene and the Fe–N bond distance was 1.875 Å. The result is consistent with the previous calculations (the Fe–N distance is around 1.87–1.89 Å[27,50]). It is noticed that the Fe–N distance of the embedded FeN_4 is generally shorter compared to that in metalmacrocyclic molecules with the FeN_4 center. *e.g.* the distance is 1.981 Å in Fe–porphyrin and 1.923 Å in Fe–phthalocyanine.[51] From the electronic structure analysis, we found that the oxidation state of Fe is Fe(II) with two net spins in the 3d orbitals of Fe. For the five coordinated $Fe(CN)N_4$ center, the structure is similar with the Fe still being in the plane of graphene. The Fe–N distance is still 1.876 Å and the Fe–CN distance is 1.846 Å.

Next, we calculated the active site structures under electrochemical conditions using the DFT/CM-MPB method, where the solvation due to the aqueous solution and the surface charging due to the increase of potential are taken into account. Because the electrocatalytic ORR is sensitive to potential, we will focus on the 0.8 V *vs.* SHE condition, which is utilized practically for ORR. At 0.8 V *vs.* SHE, the Fe–N distance is calculated to be 1.895 Å for FeN_4 and 1.883 Å for $Fe(CN)N_4$, which are slightly lengthened compared to those calculated in vacuum. Obviously, the presence of the electrochemical conditions does not alter much the structure of the active site, implying the high stability of the central FeN_4 unit.

3.2 4e reduction pathway

By using the DFT/CM-MPB method, we have first investigated the reaction channels the 4e reduction pathway following eqn (1)–(6). The free energy reaction profiles for ORR on the FeN_4 and $Fe(CN)N_4$ centers at 0.8 V *vs.* SHE have been determined, as shown in Fig. 2 and the decomposed energetics in each step are listed in Table 1.

ORR initiates by molecular O_2 adsorption on the central Fe metal (state **1**, see Fig. 2). The adsorption of O_2 on the nearby carbon and nitrogen atom sites is very weak and is thus unlikely.

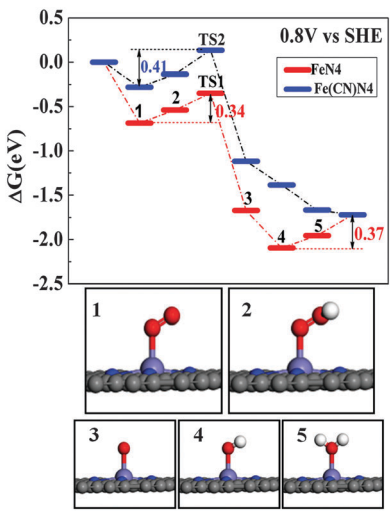

Fig. 2 The free energy profiles for the 4e ORR pathway on the embedded FeN_4 (red) and $Fe(CN)N_4$ (blue) centers at 0.8 V *vs.* SHE. **1**: O_2*; **2**: OOH*; **3**. O*; **4**. OH*; **5**. H_2O*. The free energy zero is set as that of O_2 in the gas phase (ambient condition) and the clean surface. Selected intermediate structures on the FeN_4 are also shown (the states corresponding to $Fe(CN)N_4$ are similar). The grey, blue, purple, red and white balls represent C, N, Fe, O and H, respectively.

Table 1 The free energy (ΔG) change of the elementary steps involved in the 4e reduction on the embedded FeN_4 and $Fe(CN)N_4$ centers. All energies are in eV

Elementary steps	ΔE	$\Delta H(0 \rightarrow 298\ K)$	ZPE	$-TS$	$-\lvert e\rvert U$	ΔG
FeN_4 at 0.8 V						
$O_2 \rightarrow O_2^*$	−1.33	−0.09	0.10	0.64	0.00	−0.68
$O_2^* + H^+ + e^- \rightarrow OOH^*$	−1.02	−0.05	0.22	0.20	0.80	0.15
$OOH^* \rightarrow [O\text{–}OH]^*(TS)$	0.11	0.00	−0.07	0.15	0.00	0.19
$OOH^* + H^+ + e^- \rightarrow O^* + H_2O$	−1.51	0.06	−0.01	−0.47	0.80	−1.13
$O^* + H^+ + e^- \rightarrow OH^*$	−1.58	−0.05	0.21	0.20	0.80	−0.42
$OH^* + H^+ + e^- \rightarrow H_2O^*$	−1.01	−0.05	0.20	0.20	0.80	0.14
$H_2O^* \rightarrow H_2O$	1.02	0.10	−0.22	−0.67	0.00	0.23
$Fe(CN)N_4$ at 0.8 V						
$O_2 \rightarrow O_2^*$	−0.93	−0.09	0.10	0.64	0.00	−0.28
$O_2^* + H^+ + e^- \rightarrow OOH^*$	−1.03	−0.05	0.22	0.20	0.80	0.14
$OOH^* \rightarrow [O\text{–}OH]^*(TS)$	0.19	0.00	−0.07	0.15	0.00	0.27
$OOH^* + H^+ + e^- \rightarrow O^* + H_2O$	−1.36	0.06	−0.01	−0.47	0.80	−0.98
$O^* + H^+ + e^- \rightarrow OH^*$	−1.43	−0.05	0.21	0.20	0.80	−0.27
$OH^* + H^+ + e^- \rightarrow H_2O^*$	−0.87	−0.05	0.20	0.20	0.80	−0.28
$H_2O^* \rightarrow H_2O$	0.84	0.10	−0.22	−0.67	0.00	0.05

For the O_2 adsorption on Fe, two possible O_2 configurations were examined, namely, the end-on and the side-on configurations.[52] The end-on configuration has only one oxygen atom directly bonded with the Fe with the O–O axis tilted away from the Fe–N plane, while the side-on configuration have both O atoms bonded with the Fe with the O–O axis in parallel with the Fe–N plane. We found that on both FeN_4 and $Fe(CN)N_4$ catalysts, the end-on configuration is preferred energetically, which is different from O_2 adsorption on the Pt surface where the side-on configuration is generally preferred.[45] The O_2 adsorption free energy is 0.68 eV on the FeN_4, and drops to 0.28 eV on the $Fe(CN)N_4$ (see Table 1). Our Mulliken charge analysis showed that the adsorbed O_2 on both Fe centers accumulates electrons to form superoxo O_2 ion, also evident from the lengthened O–O distance (1.28 Å) compared to the gas phase O_2 molecule. The charge depletion occurs not only at the Fe center, but also at the nearby carbon sites of the graphene, indicating the transfer of the Fermi electron of the graphene to the antibonding states of the O_2 molecule.

We noted that the O_2 adsorption on similar FeN_4 structures have been reported in previous theoretical calculations. For example, on the iron phthalocyanine molecule, O_2 adsorbs with the end-on configuration and has an adsorption energy of 1.16 eV;[53] on the FeN_4 embedded in the carbon nanotube (18, 0), the O_2 adsorption energy is calculated to be 1.06 eV.[23] Considering that these calculations have a different catalyst model from this work and generally did not include the solvation environment, the calculated adsorption energy on FeN_4 (ΔE = 1.33 eV including the solvation) here agree reasonably with the previous data. This also indicates that the electronic structure of the FeN_4 center at different chemical environments is quite similar (*e.g.* Fe^{2+}).

The lower adsorption energy of O_2 on the $Fe(CN)N_4$ center is interesting, suggesting that the increased coordination of Fe will reduce the adsorption energy of O_2. Due to the strong coordination ability of the CN ligand (CN^-), we found that the oxidation state of the center Fe in $Fe(CN)N_4$ is raised to 3^+ (Fe(III)). Compared to Fe(II), the Fe(III) has a low ability to donate electrons to the antibonding $2\pi^*$ orbitals of O_2 and thus the bonding of Fe–O_2 is weakened, as also evident from the calculated Fe–O_2 distances: 1.871 Å in FeN_4 and 2.152 Å in $Fe(CN)N_4$.

The adsorbed O_2 can be easily hydrogenated at 0.8 V to the adsorbed OOH, $O_2^* + H^+ + e^- \rightarrow OOH^*$, once a solvated proton approaches the adsorbed O_2, as shown in Fig. 2. This step is slightly uphill in the energy profile by ∼0.15 eV on both catalysts and the calculated free energy barrier is also ∼0.15 eV (after ZPE correction, see ESI,† Fig. S1 for the located (IS), TS and FS structures). The O–O bond of OOH* is lengthened to 1.439 Å and 1.451 Å on the FeN_4 and $Fe(CN)N_4$ centers, respectively, which is already similar to that in the free H_2O_2 molecule (1.470 Å).

The key step in the 4e reduction pathway is the O–O bond breaking as written in eqn (3), which occurs by breaking the O–O bond of the adsorbed OOH (state 2). In this step, a solvated proton above the OOH helps to accept the dissociated OH. Overall, the reaction involves the coupled proton–electron transfer to form H_2O and the breaking of the O–O bond, $OOH^* + H^+ + e^- \rightarrow O^* + H_2O$. The located initial state (IS), the TS and the final state (FS) of this step on both Fe catalysts are depicted in Fig. 3. At the IS, the presence of solvated proton $H_3O^+(H_2O)$ helps to increase the O–O bond of OOH, 1.502 Å for FeN_4 and 1.488 Å for $Fe(CN)N_4$. At the TS, the O–O bond of OOH

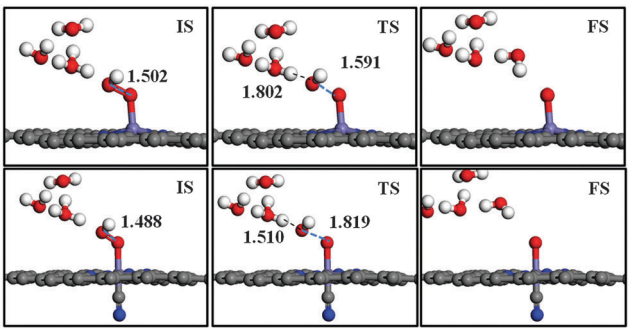

Fig. 3 The IS, TS and FS structures of the O–O bond breaking step ($OOH^* + H^+ + e^- \rightarrow O^* + H_2O$) on FeN_4 (top panel) and $Fe(CN)N_4$ (bottom panel). The labeled distances are in Å.

is further lengthened, 1.591 Å for FeN_4 and 1.819 Å for $Fe(CN)N_4$, and the leaving OH group starts to evolve bonding with the H of the solvated proton. It is noticed that the solvated proton is still quite far away from the OH of the [O–OH] TS complex (>1.5 Å), indicating the weak interaction of the [O–OH] TS complex with the solvated proton. After the TS, the solvated proton quickly approaches the OH that forms a H_2O molecule in the solution and leaves a terminal O on the Fe center. From Fig. 2, it is clear that the TS of O–O bond breaking dictates the highest free energy position along the whole 4e reduction pathway and thus this reaction is a key kinetic step in the 4e reduction. The calculated free energy barrier is 0.34 eV on FeN_4 with respect to the adsorbed O_2 molecule (state **1**), which is 0.07 eV lower than that on $Fe(CN)N_4$.

It should be emphasized that the O–O bond breaking mechanism for ORR on the FeN catalysts is different from those identified for ORR on extended Pt surfaces.[45,52] On Pt surfaces, the O–O bond breaking follows either the O–O direct dissociation or the O–OH dissociation, involving at least two surface Pt atoms. In particular, the solvated proton is not required to act as a reactant to accept the O or OH after the O–O bond breaking. By contrast, the O–O bond breaking on the Fe centers follows only the O–OH dissociation and the solvated proton reacts with the dissociated OH to form water. Obviously, the difference is due to the nature of the reaction sites: for the reaction on the Fe center, there is no extra metal site for the adsorption of the dissociated O or OH, unlike the reaction occurring on Pt surfaces. Indeed, for O_2 direct dissociation, we found that the dissociated O atoms on FeN_4 is 0.87 eV less stable than the initial O_2 adsorption state and this data is 2.01 eV on $Fe(CN)N_4$ (the structures of the dissociated O atoms are shown in ESI,† Fig. S2). The large endothermic reaction energies indicate that O_2 direct dissociation is unlikely on these mono-Fe center sites.

Next, the adsorbed terminal O* can be stepwisely hydrogenated to OH and to H_2O *via* the coupled proton and electron transfer. We have searched for the TSs of these two steps and found that the barriers are less than 0.1 eV on both Fe catalysts. On the FeN_4 center, the free energy change from the adsorbed OH* to H_2O in solution is 0.37 eV, which is comparable to the barrier of the O–OH bond breaking (0.34 eV). This indicates that the presence of an additional OH on the FeN_4 center is highly likely at the 0.8 V condition, both thermodynamically and kinetically. The presence of OH should not poison the FeN_4 center, *i.e.* $Fe(OH)N_4$ center, since the ORR can also occur on the five coordinated $Fe(CN)N_4$, as shown in Fig. 2. On the $Fe(CN)N_4$ center, the reduction of O to OH and to H_2O is downhill energetically, suggesting the five coordinated Fe center is thermodynamically more stable at the 0.8 V condition.

3.3 2e reduction pathway

In parallel with the 4e reduction pathway, the 2e reduction leading to H_2O_2 may also occur, which is a bifurcated route from the 4e reduction at the stage of the adsorbed OOH (see eqn (7) and (8)). The O-end of the OOH is hydrogenated to H_2O_2, which then desorbs to solution to complete the 2e

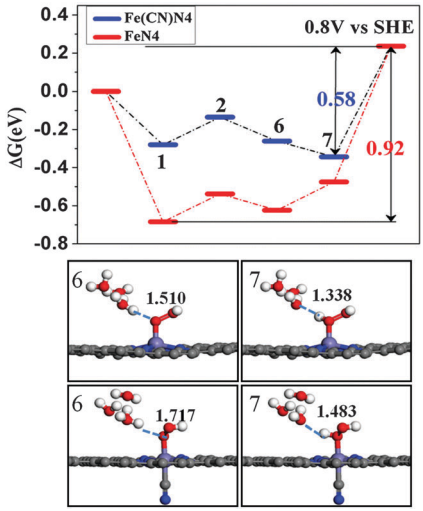

Fig. 4 Free energy profile for the 2e reduction pathway from O_2 to H_2O_2 on the embedded FeN_4 (red) and $Fe(CN)N_4$ (blue) centers at 0.8 V *vs.* SHE. **1**: O_2*; **2**: OOH*; **6**: OOH* with solvated proton; **7**: H_2O_2* with H_2O (the first solvation shell). The labeled distances are in Å.

reduction. Using DFT/CM-MPB method, we have investigated this 2e reduction pathway on both Fe catalysts and the free energy profile is shown in Fig. 4.

The overall mechanism of the 2e reduction pathway is summarized as follows. At the 0.8 V condition, the adsorbed OOH can first interact with an incoming solvated proton to form a metastable [H_2OH–OOH] complex, as shown in the state **6** of Fig. 4. Next, the adsorbed H_2O_2 (state 7) is formed by the coupled proton and electron transfer from the [H_2OH–OOH] complex. The TSs for the hydrogenation (**6** → **7**) have been located (see ESI,† Fig. S3) and the free energy barriers are calculated to be 0.15 eV on FeN_4 and ~0 eV (after ZPE correction) on $Fe(CN)N_4$. The adsorbed H_2O_2 is found to interact strongly with the nearby H_2O molecules, indicating that the first solvation shell is critical for the stability of H_2O_2 on the Fe centers. The 2e reduction ends when the adsorbed H_2O_2 is released to solution.

From the free energy profile in Fig. 4, we can conclude that the desorption of the adsorbed H_2O_2 is the rate-determining step in the 2e reduction. The overall barrier from the adsorbed O_2 to the H_2O_2 in solution is 0.92 eV on the FeN_4, and it is 0.58 eV on the $Fe(CN)N_4$. Compared with the energetics of the 4e reduction pathways (Fig. 2), we found that the 2e reduction is kinetically unlikely on the FeN_4 center (the overall barrier is more than 0.5 eV higher than that in the 4e reduction), while it is likely with the 4e reduction on the $Fe(CN)N_4$ with the difference of the overall barriers of the two routes being around 0.17 eV (see the overall mechanism summarized in ESI,† Fig. S4).

It might be mentioned that H_2O_2 dissociation into two OH groups has also been considered on the FeN_4 site, which, if it occurs, will revert the reaction back to the 4e reduction (on the $Fe(CN)N_4$ site it is not possible for H_2O_2 dissociation because two OH groups on the Fe site will spontaneously combine to

form H_2O_2 after optimization). We found that the solvation plays an important role to stabilize the adsorbed H_2O_2 molecule on the FeN_4 center. Without the explicit solvation ($(H_2O)_3$ nearby the H_2O_2 molecule), the adsorbed H_2O_2 can spontaneously dissociate into two OH groups on FeN_4. Previously, Chen *et al.* also found that for H_2O_2 adsorption on Fe–phthalocyanine in vacuum, H_2O_2 will dissociate and the O–O distance of the product is 2.368 Å.[49] By contrast, with the explicit solvation, the O–O bond breaking of H_2O_2 on FeN_4 needs to overcome a barrier of 0.42 eV. Therefore, the overall barrier for the 4e pathway *via* H_2O_2 dissociation is 0.63 eV with respect to the adsorbed O_2 molecule (state **1**), which is also much higher than the pathway *via* OOH dissociation (0.37 eV, Fig. 2). Therefore, the ORR pathways *via* H_2O_2 intermediate are kinetically unfavorable on the FeN_4 site (see the overall mechanism summarized in ESI,† Fig. S4).

4. Discussion on the kinetics

Our results show that the one-electron reduction from OH to H_2O on the FeN_4 center has a similar or even higher barrier than that of the O–OH bond breaking. The adsorption of OH on the four-coordinated Fe is thermodynamically favored at the working potentials, which can be produced readily by water dissociation in the aqueous environment of ORR. Since the Fe/N/C catalysts are generally prepared at high temperatures, we expect that the four-coordinated Fe as the active site is highly unlikely, both thermodynamically and kinetically: the stand alone FeN_4 structure can be readily terminated by a fifth ligand in the experimental conditions, such as CN in the catalyst preparation stage, or OH in the ORR conditions. We therefore will mainly focus on the results obtained on the $Fe(CN)N_4$ structure and compare its kinetics with the experimental findings.

We are now in a position to discuss the potential dependent ORR kinetics on the $Fe(CN)N_4$ centers. Fig. 2 shows that the TS of the O–OH bond breaking in the 4e reduction pathway dictates the highest energy position in the free energy profile. The overall barrier height for the O–OH bond breaking at 0.8 V is constituted of two parts, (i) the free energy change from O_2 to OOH, $O_2^* + H^+ + e^- \rightarrow OOH^*$; and (ii) the free energy barrier of the OOH dissociation, $OOH^* + H^+ + e^- \rightarrow O^* + H_2O$. The step (i) can be treated as a fast equilibrium with the ΔG being 0.14 eV at 0.8 V for $Fe(CN)N_4$ (see Table 1). Because this step involves explicitly one electron transfer, ΔG should vary upon the change of potential according to $\Delta G = \Delta G|_{0.8V} + |e|(U - 0.8)$. Therefore, 0.66 V is the equilibrium potential between the adsorbed O_2 and the adsorbed OOH. Below 0.66 V, the overall barrier of O–OH bond breaking should be only determined by the free energy barrier of the (ii) step, the OOH dissociation.

For the step (ii), a TS to break O–OH bond is present and therefore whether the OOH dissociation is potential dependent is related to the nature of the TS. From the optimized TS structure shown in Fig. 3, we noticed that the TS is in fact IS-like and the solvated proton links with the dissociating O–OH complex *via* hydrogen bonding. This implies that the solvated proton acts largely as a spectator to stabilize the TS and the electron is not transferred yet at the TS. If so, the OOH dissociation step on the Fe centers is not sensitive to the potential condition. Indeed, we have checked the potential dependency of the OOH dissociation over the $Fe(CN)N_4$ using the constant-charge DFT/CM-MPB method[54] (our previous work shows that the PBE functional of DFT is able to describe reasonably the potential dependent activity for reactions on metallic surfaces[39]). Our results show that the barrier remains quite constant over the potential range investigated, as shown in Fig. 5.

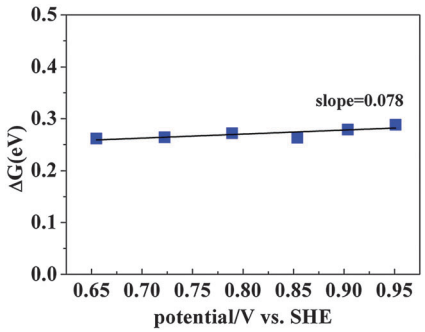

Fig. 5 The plot of free energy barrier ΔG_a (eV) of the O–OH bond breaking against the potential on $Fe(CN)N_4$.

By summing the two steps from the adsorbed O_2 to dissociated O, we can deduce that the kinetics of the O–O bond breaking on the Fe centers are potential dependent ($\Delta G_a = \Delta G_a^0 - \alpha F\eta$) with the apparent charge transfer coefficient, α, being 1 above 0.66 V, which is owing to the one-electron reduction from O_2 to OOH. The theoretical Tafel slope ($b = 2.3RT/\alpha F$) can thus be computed to be around 60 mV decade^{-1}. It is interesting to compare our theoretical Tafel slope for the O–OH bond breaking with the experimental data on ORR kinetics. Jaouen *et al.* have investigated nine non-noble-metal catalysts for ORR in acidic media and the measured Tafel slopes are generally within the range of 54–65 mV decade^{-1} at the interval 0.9–0.75 V *vs.* RHE.[55] Chlistunoff *et al.* investigated the Tafel behavior on Fe/N/C catalyst prepared by the pyrolysis of Fe/polyaniline and carbon black. They found that the Tafel slope switches from 60 mV at low overpotentials to more than 240 mV at high overpotentials[56] and the change of the Tafel slope occurs around 0.65 V. From our results, the increase of the Tafel slope at high overpotentials could be understood as the consequence of the O_2/OOH equilibrium favoring the OOH and the overall barrier is only contributed from the O–OH bond breaking of OOH that is not a potential sensitive reaction. It is also likely that at the high overpotential conditions the diffusion of the reactants might turn out to be kinetically important.

From the obtained reaction network, we can utilize microkinetics to estimate the reaction rate of the 4e and the 2e reduction pathways on the five-coordinated $Fe(CN)N_4$. Our results show that both 4e and 2e reduction pathways are likely: the H_2O is the major product and the H_2O_2 is the by-product. Because the reaction channel to H_2O has an overall barrier of 0.41 eV, which is 0.17 eV lower than that of the H_2O_2 formation, one can estimate that the 2e reduction pathway contributes only 0.1% in the total O_2 reduction assuming the reaction

temperature is 300 K and the two channels have the same pre-exponential factor.

Our results suggest that the five-coordinated $Fe(CN)N_4$ are good catalysts for ORR with a high selectivity to the 4e reduction pathway. The calculated barrier at 0.8 V is around 0.4 eV, which is about 0.2 eV lower than those determined on the Pt(111) surface within the same theoretical framework.[45] This indicates that the non-Pt catalyst could have a higher catalytic activity per active site. Therefore, the major concern in practice should be the efficient implantation of the FeN_4 center into the graphene plane to achieve a high concentration of the active centers in the Fe/N/C catalysts.

5. Conclusion

This work represents a theoretical survey on the reaction mechanism of the electrocatalytic ORR over two possible non-Pt catalyst model, namely the four coordinated FeN_4 and five coordinated $Fe(CN)N_4$ structures that are embedded inside the graphene plane. These two theoretical models in heterogeneous environment mimic those in the Fe-containing complex in homogeneous catalysis. Both the 4e and 2e reduction over the FeN centers have been investigated at the working potential conditions. Theoretical results show that both the FeN_4 center and the $Fe(CN)N_4$ center can be good catalysts for ORR with a low activation barrier and a good selectivity to 4e reduction. The presence of five coordinated $Fe(X)N_4$ (X = CN or OH) is more likely thermodynamically due to strong bonding of Fe towards the fifth ligand. The major challenge in practice is the creation of such active centers with a high concentration. Our major results are outlined as follows.

(i) The four-coordinated FeN_4 center can bond the reaction intermediates, such as the O_2, OOH, OH species more strongly compared to the five-coordinated $Fe(CN)N_4$ center. The Fe center is Fe(II) in the FeN_4 and is Fe(III) in the $Fe(CN)N_4$.

(ii) The 4e reduction pathway follows the $O_2 \rightarrow OOH \rightarrow O \rightarrow OH \rightarrow H_2O$ mechanism. On the FeN_4 center, the O–OH bond breaking and the OH reduction at 0.8 V have a similar overall free energy barrier, being 0.34 and 0.37 eV, respectively. On the $Fe(CN)N_4$ center, the O–OH bond breaking is the rate-determining step with the free energy barrier being 0.41 eV.

(iii) The 2e reduction pathway follows the $O_2 \rightarrow OOH \rightarrow H_2O_2$ mechanism. On the FeN_4 center, due to the high adsorption energy of O_2, the 2e reduction channel is unlikely with a high overall barrier, 0.92 eV. On the $Fe(CN)N_4$ center, the 2e reduction is possible with the overall barrier being 0.58 eV.

(iv) The ORR kinetics on the $Fe(CN)N_4$ centers are potential dependent with the theoretical Tafel slope being 60 mV above $\sim$0.66 V, involving the coupled proton–electron transfer from O_2 to OOH. The O–O bond breaking of OOH is not potential dependent with the solvated proton nearby behaving like a spectator at the TS at the potentials investigated.

Acknowledgements

We acknowledge the National Science Foundation of China (21173051, 21361130019, 21103110), 973 program (2011CB808500, 2013CB834603), Science and Technology Commission of Shanghai Municipality (08DZ2270500), and Program for Professor of Special Appointment (Eastern Scholar) at Shanghai Institute of Higher Learning, China and Shanghai Postdoctoral Science Foundation (2012M520040, 2013T60413, 12R21411200) and Innovation Program of Shanghai Municipal Education Commission (13YZ120) for financial support.

References

1 Y. Dai, L. Ou, W. Liang, F. Yang, Y. Liu and S. Chen, *J. Phys. Chem. C*, 2011, **115**, 2162–2168.
2 H. A. Gasteiger and N. M. Marković, *Science*, 2009, **324**, 48–49.
3 J. Greeley and J. K. Nørskov, *J. Phys. Chem. C*, 2009, **113**, 4932–4939.
4 R. Jasinski, *Nature*, 1964, **201**, 1212–1213.
5 G. Wu, C. M. Johnston, N. H. Mack, K. Artyushkova, M. Ferrandon, M. Nelson, J. S. Lezama-Pacheco, S. D. Conradson, K. L. More, D. J. Myers and P. Zelenay, *J. Mater. Chem.*, 2011, **21**, 11392–11405.
6 H. Xiao, Z. G. Shao, G. Zhang, Y. Gao, W. T. Lu and B. L. Yi, *Carbon*, 2013, **57**, 443–451.
7 E. Proietti, F. Jaouen, M. Lefèvre, N. Larouche, J. Tian, J. Herranz and J.-P. Dodelet, *Nat. Commun.*, 2011, **2**, 416.
8 M. Lefevre, E. Proietti, F. Jaouen and J. P. Dodelet, *Science*, 2009, **324**, 71–74.
9 F. Jaouen, F. Charreteur and J. P. Dodelet, *J. Electrochem. Soc.*, 2006, **153**, A689–A698.
10 F. Jaouen and J.-P. Dodelet, *Electrochim. Acta*, 2007, **52**, 5975–5984.
11 G. Faubert, R. Côté, D. Guay, J. P. Dodelet, G. Dénès, C. Poleunis and P. Bertrand, *Electrochim. Acta*, 1998, **43**, 1969–1984.
12 H. Schulenburg, S. Stankov, V. Schünemann, J. Radnik, I. Dorbandt, S. Fiechter, P. Bogdanoff and H. Tributsch, *J. Phys. Chem. B*, 2003, **107**, 9034–9041.
13 S. Baranton, C. Coutanceau, C. Roux, F. Hahn and J. M. Léger, *J. Electroanal. Chem.*, 2005, **577**, 223–234.
14 R. Baker, D. P. Wilkinson and J. Zhang, *Electrochim. Acta*, 2008, **53**, 6906–6919.
15 E. Yeager, *J. Mol. Catal.*, 1986, **38**, 5–25.
16 J. P. Collman, P. Denisevich, Y. Konai, M. Marrocco, C. Koval and F. C. Anson, *J. Am. Chem. Soc.*, 1980, **102**, 6027–6036.
17 E. Yeager, *Electrochim. Acta*, 1984, **29**, 1527–1537.
18 U. I. Koslowski, I. Abs-Wurmbach, S. Fiechter and P. Bogdanoff, *J. Phys. Chem. C*, 2008, **112**, 15356–15366.
19 A. L. Bouwkamp-Wijnoltz, W. Visscher, J. A. R. van Veen, E. Boellaard, A. M. van der Kraan and S. C. Tang, *J. Phys. Chem. B*, 2002, **106**, 12993–13001.
20 R. W. Joyner, J. A. R. van Veen and W. M. H. Sachtler, *J. Chem. Soc., Faraday Trans. 1*, 1982, **78**, 1021–1028.
21 M. Lefèvre, J. P. Dodelet and P. Bertrand, *J. Phys. Chem. B*, 2000, **104**, 11238–11247.
22 J. Yang, D.-J. Liu, N. N. Kariuki and L. X. Chen, *Chem. Commun.*, 2008, 329–331.

23 D. H. Lee, W. J. Lee, W. J. Lee, S. O. Kim and Y.-H. Kim, *Phys. Rev. Lett.*, 2011, **106**, 175502.
24 M. Lefèvre, J. P. Dodelet and P. Bertrand, *J. Phys. Chem. B*, 2002, **106**, 8705–8713.
25 U. I. Kramm, J. Herranz, N. Larouche, T. M. Arruda, M. Lefevre, F. Jaouen, P. Bogdanoff, S. Fiechter, I. Abs-Wurmbach, S. Mukerjee and J. P. Dodelet, *Phys. Chem. Chem. Phys.*, 2012, **14**, 11673–11688.
26 F. Calle-Vallejo, J. I. Martinez and J. Rossmeisl, *Phys. Chem. Chem. Phys.*, 2011, **13**, 15639–15643.
27 S. Kattel and G. Wang, *J. Mater. Chem. A*, 2013, **1**, 10790–10797.
28 J. Herranz, M. Lefèvre, N. Larouche, B. Stansfield and J.-P. Dodelet, *J. Phys. Chem. C*, 2007, **111**, 19033–19042.
29 G. Wu, K. L. More, C. M. Johnston and P. Zelenay, *Science*, 2011, **332**, 443–447.
30 M. Jain, S.-h. Chou and A. Siedle, *J. Phys. Chem. B*, 2006, **110**, 4179–4185.
31 S. Chatterjee, K. Sengupta, S. Samanta, P. K. Das and A. Dey, *Inorg. Chem.*, 2013, **52**, 9897–9907.
32 L. Capece, M. A. Marti, A. Crespo, F. Doctorovich and D. A. Estrin, *J. Am. Chem. Soc.*, 2006, **128**, 12455–12461.
33 J. M. Soler, E. Artacho, J. D. Gale, A. Garcia, J. Junquera, P. Ordejon and D. Sanchez-Portal, *J. Phys.: Condens. Matter*, 2002, **14**, 2745–2779.
34 J. Junquera, Ó. Paz, D. Sánchez-Portal and E. Artacho, *Phys. Rev. B: Condens. Matter*, 2001, **64**, 235111.
35 N. Troullier and J. L. Martins, *Phys. Rev. B: Condens. Matter*, 1991, **43**, 1993–2006.
36 J. P. Perdew, K. Burke and M. Ernzerhof, *Phys. Rev. Lett.*, 1996, **77**, 3865–3868.
37 H.-F. Wang and Z.-P. Liu, *J. Am. Chem. Soc.*, 2008, **130**, 10996–11004.
38 C. Shang and Z.-P. Liu, *J. Chem. Theory Comput.*, 2010, **6**, 1136–1144.
39 Y.-H. Fang and Z.-P. Liu, *J. Am. Chem. Soc.*, 2010, **132**, 18214–18222.
40 Y.-F. Li, Z.-P. Liu, L. Liu and W. Gao, *J. Am. Chem. Soc.*, 2010, **132**, 13008–13015.
41 *CRC Handbook of Chemistry and Physics*, ed. D. R. Lide, CRC press, 2003–2004.
42 Z.-P. Liu, S. J. Jenkins and D. A. King, *J. Am. Chem. Soc.*, 2004, **126**, 10746–10756.
43 J. O. M. Bockris and S. U. Khan, *Surface Electrochemistry: A Molecular Level Approach.*, Plenum Press, New York, 1993.
44 J. Rossmeisl, A. Logadottir and J. K. Nørskov, *Chem. Phys.*, 2005, **319**, 178–184.
45 G.-F. Wei, Y.-H. Fang and Z.-P. Liu, *J. Phys. Chem. C*, 2012, **116**, 12696–12705.
46 S. Gupta, D. Tryk, I. Bae, W. Aldred and E. Yeager, *J. Appl. Electrochem.*, 1989, **19**, 19–27.
47 S. Gupta, C. Fierro and E. Yeager, *J. Electroanal. Chem.*, 1991, **306**, 239–250.
48 C.-W. Tsai, H. M. Chen, R.-S. Liu, K. Asakura, L. Zhang, J. Zhang, M.-Y. Lo and Y.-M. Peng, *Electrochim. Acta*, 2011, **56**, 8734–8738.
49 R. Chen, H. Li, D. Chu and G. Wang, *J. Phys. Chem. C*, 2009, **113**, 20689–20697.
50 A. Titov, P. Zapol, P. Král, D.-J. Liu, H. Iddir, K. Baishya and L. A. Curtiss, *J. Phys. Chem. C*, 2009, **113**, 21629–21634.
51 Z. Shi and J. Zhang, *J. Phys. Chem. C*, 2007, **111**, 7084–7090.
52 Z. Shi, H. Liu, K. Lee, E. Dy, J. Chlistunoff, M. Blair, P. Zelenay, J. Zhang and Z.-S. Liu, *J. Phys. Chem. C*, 2011, **115**, 16672–16680.
53 G. F. Wang, N. Ramesh, A. Hsu, D. Chu and R. R. Chen, *Mol. Simul.*, 2008, **34**, 1051–1056.
54 Y.-H. Fang, G.-F. Wei and Z.-P. Liu, *J. Phys. Chem. C*, 2014, **118**, 3629.
55 F. d. r. Jaouen, J. Herranz, M. Lefèvre, J.-P. Dodelet, U. I. Kramm, I. Herrmann, P. Bogdanoff, J. Maruyama, T. Nagaoka, A. Garsuch, J. R. Dahn, T. Olson, S. Pylypenko, P. Atanassov and E. A. Ustinov, *ACS Appl. Mater. Interfaces*, 2009, **1**, 1623–1639.
56 J. Chlistunoff, *J. Phys. Chem. C*, 2011, **115**, 6496–6507.

